ELSEVIER

Journal of Fluids and Structures 24 (2008) 907–919

JOURNAL OF FLUIDS AND STRUCTURES

www.elsevier.com/locate/jfs

Two-degree-of-freedom vortex-induced vibrations of a spring-mounted rigid cylinder with low mass ratio

A. Sanchis, G. Sælevik, J. Grue*

Mechanics Division, Department of Mathematics, University of Oslo, P.O. Box 1053, Blindern, NO-0316 Oslo, Norway

Received 5 April 2006; accepted 11 December 2007
Available online 4 March 2008

Abstract

This work studies the vortex-induced vibrations of an elastically mounted rigid cylinder able to move in-line and transverse to the flow, with equal mass ratio and natural frequencies in both directions. A compact and simple set-up using torsion springs was designed for this purpose. Although the mass ratio is close to 1, the mass-damping parameter α is high enough so that the system exhibits a two-branch type response. Consequently, the 'super-upper' branch is not observed, and the peak transverse response is unaffected compared to transverse-only oscillations. We also note that measurement points associated with a '2S' mode of vortex formation are found in the '2P' area of the map of vortex regimes. This discrepancy is discussed in light of the influence of streamwise motion on the critical curve separating the '2S' and '2P' regimes.

Keywords: Vortex-induced vibrations; In-line and cross-flow response; Critical curve

1. Introduction

Vortex-induced-vibrations (VIV) cause problems in many areas related to offshore engineering, particularly to the design of the risers and pipelines in free spans. Recent model tests on free-spanning pipelines made for the Ormen Lange development project have shown that the combined cross-flow and in-line motions are important. This means that an analysis where the in-line motion is disregarded is found to be insufficient. Other previous tests have revealed that the in-line VIV contributes equally much to fatigue as cross-flow VIV. Furthermore, there is an interaction between the two degrees of freedom, so they cannot be simply superimposed. This is indeed the case when there is an initial sag as on a pipeline in free span. A combined in-line and cross-flow motion, in high Reynolds number flow, represents an important challenge relevant to fundamental understanding as well as to engineering practice. The Reynolds number in the present experiments is above 1×10^4.

The research accomplished in the past three decades on VIV has been reviewed in Williamson and Govardhan (2004). Up to 2004, a majority of studies focused on transverse oscillations only. In the case of the free oscillations of elastically mounted rigid cylinders, the amplitude and frequency response was thoroughly investigated by Govardhan and Williamson (2000), who emphasized the distinction between high and low mass-damping systems. In the course of our work, two relevant papers have been published that extend this analysis. With help of a magnetic eddy current damping

*Corresponding author.
E-mail addresses: arnauds@math.uio.no (A. Sanchis), gsalevik@math.uio.no (G. Sælevik), johng@math.uio.no (J. Grue).

0889-9746/$ - see front matter © 2008 Elsevier Ltd. All rights reserved.
doi:10.1016/j.jfluidstructs.2007.12.008

system, Klamo et al. (2006) studied the influence of the structural damping ζ on the different response branches, separately from the mass ratio m^*. The ground-breaking work by Govardhan and Williamson (2006) is also based on damping control: being able to impose both negative and positive mechanical damping on their system, the authors revealed that the peak-amplitude response depends exclusively on the Reynolds number and the mass-damping parameter α. They proposed a functional relation of the form $A^* = g(\alpha)f(\mathrm{Re})$ and defined a 'modified' Griffin plot where peak amplitudes A^*_M are now independent of the Reynolds number. This procedure was found to collapse together a large number of peak-amplitude data that were previously scattered in the traditional Griffin plot.

Early two-degree-of-freedom experiments combining cross-flow and streamwise oscillations suggested that the ability of the system to move in the streamwise direction has little effect on the system response. In Moe and Wu (1990), a cylinder was attached to a rig functioning as a parallelogram, and the in-line motion could be either restrained or spring-supported. The mass ratios were very different in the two directions and the natural frequency ratio was set to $f_X/f_Y = 2.18$. Slightly higher amplitudes were found in presence of the in-line motion, and transverse force measurements along the span indicated a better correlation. A different mounting was used in the work by Sarpkaya (1995) with two bearing systems riding on top of each other. Here also the mass ratios were quite different in the two directions, but the natural frequencies could be adjusted. For $f_X = f_Y$, the amplitude was increased by 20% compared to the transverse-only case.

A set of two-degree-of-freedom results was presented in Pesce and Fujarra (2002) for a cantilevered rigid cylinder connected to an elastic support, with adjustable natural frequencies f_X and f_Y and a mass ratio almost similar in the two directions ($m^* = 10$ and 13). The amplitude response showed evidence of the different branches, and once again the effect of streamwise oscillations was limited to a small increase in the transverse response.

In their forced-oscillations experiments, Jeon and Gharib (2001) studied the effect of streamwise oscillations on the near-wake, in relation to the experiments by Williamson and Roshko (1988) for transverse-only oscillations. They found that in the '2P' vortex regime, the additional vortex composing each pair was inhibited by the in-line oscillations, although the phase shift in the primary vortex shedding was still observed. For the '2S' mode, an increase in the coherence of the vortex shedding was noted, in agreement with the observations by Moe and Wu (1990).

A comprehensive study on the response of a rigid, elastically mounted cylinder in two degrees of freedom (2-dof) was presented by Jauvtis and Williamson (2004), with equivalent mass ratios and natural frequencies in both directions and a low structural damping. An ingenious solution was developed to satisfy these conditions: the vertical cylinder was suspended to the roof by long cables like a pendulum, and gravity acted as the restoring force. Consistently with the previous works, 2-dof motion resulted in a marginal increase in the transverse response for moderate mass ratios, greater than 6. For $m^* < 6$, however, the system response was drastically modified: the upper branch was replaced by a new response branch (denoted 'super-upper') characterized by different vortex dynamics and transverse amplitudes reaching 3 diameters peak-to-peak! These results, of major implication for the design of numerical codes predicting VIV, were confirmed by Pesce and Fujarra (2005) in the case of a flexible cantilevered cylinder with low mass ratio and low structural damping. Such amplitudes were also found in Tryantafyllou et al. (2004) for a flexible cylinder with pinned ends towed in a tank.

We here present observations from a laboratory campaign on VIV. The experiments were set up to address some particular challenges that were communicated from industry. The experiments are designed with a moored rigid cylinder section that can oscillate in two degrees of freedom—cross-wise and in-line—while moving forward with constant speed in a wave tank where the water is otherwise at rest. Requirements included a mass ratio close to unity ($m^* = 1.04$), and that the mass-spring system has the same mass coefficient and natural frequency in the two directions of motion. The Reynolds number range was 13 000−18 600. An original and compact set-up was designed to satisfy these constraints, making use of torsion springs instead of linear springs. The investigation focuses on the cylinder response in amplitude and frequency, and the analysis is supported by flow measurements in the near-wake using particle image velocimetry (PIV).

2. Experimental set-up

2.1. Oscillating system

Experiments were carried out in a 25 m long water towing tank, with 51 cm width and 81 cm depth. Fig. 1 shows a side view of the mounting. A rigid, hollow circular cylinder made of plexiglas (span $L = 47.5$ cm, diameter $d = 8$ cm, corresponding aspect ratio $AR \simeq 6$) is suspended at each end to three torsion springs, placed around it on 10 mm-thick supporting plates. Both plates are mounted vertically on a rigid rig towed along the tank, allowing the cylinder to undergo vortex-induced oscillations in an $X-Y$ plane.

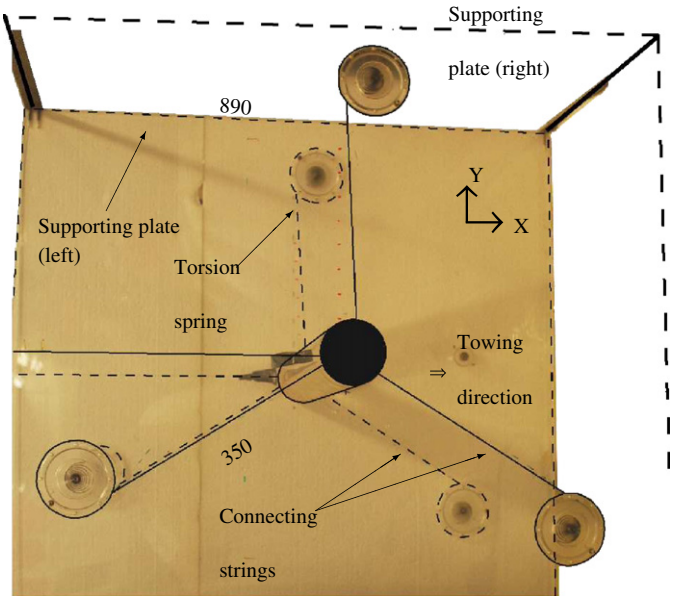

Fig. 1. Side view of the experimental set-up, showing the disposition of the plate springs around the cylinder.

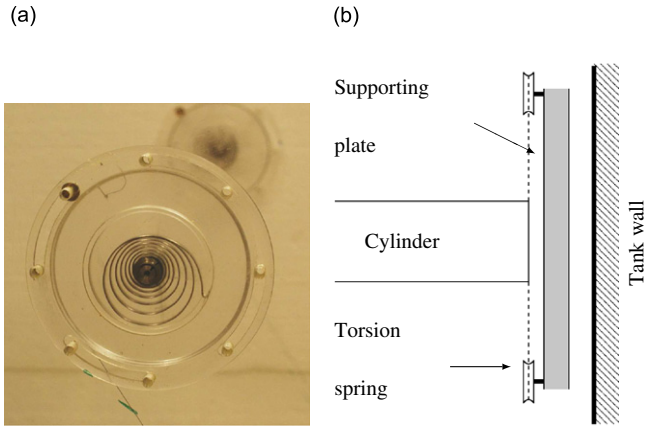

Fig. 2. (a) Close-up on a torsion spring. Wheel radius is 36 mm, nominal stiffness 12.5 N m^{-1} for one spring. (b) Front view of the mounting, showing the disposition of the supporting plate. The gap between the cylinder edge and the plate is 4 mm, and 5 mm between the plate and the side wall of the tank.

When submerged in the tank, the hollow cylinder fills with water, yielding a mass ratio m^* very close to unity. Thirty-five cm long inextensible wires connect the cylinder to the plate springs, which have a wheel radius of 3.6 cm. The arrangement of the springs is adjusted so that, for any small displacement in the $X-Y$ plane, the restoring force points towards the position of equilibrium with the same constant k, regardless of direction. For excursions larger than one diameter the direction of the spring force depends on the actual position of the cylinder with respect to the springs. This results in a slight asymmetry in the cylinder motion, with one lobe of the figure-of-eight being somewhat larger than the other. However, the time traces of the horizontal and vertical displacements presented in Fig. 3 do not reveal any significant subharmonic response resulting from the coupling between the two degrees of freedom.

It should be noted that the cylinder is *not* restrained to move in translation in the $X-Y$ plane only although these are the motions of interest here. It can as well rotate in roll and pitch motions around the X and Y axes. In order to limit contacts with the supporting plates, a 4 mm gap separates the cylinder edges from the plates (see Fig. 2).

The relatively small aspect ratio raises questions about the importance of end effects to the global results in these experiments. The limited aspect ratio increases the spanwise coordination of the vortex shedding by suppressing

cross-flow along the cylinder axis in the vicinity of the plates. However, in the study by Szepessy and Bearman (1992) it was shown that for Reynolds numbers of interest here ($\mathrm{Re} = 1.3-1.9 \times 10^4$) the fluctuating lift coefficient c'_L increased only by 12% for $\mathrm{AR} = 6$ compared to $\mathrm{AR} = 11$. Furthermore, c'_L was found to be almost constant along the span. Thus, one can expect that the impact of an aspect ratio of 6 on the VIV response of the cylinder is minimal. A confirmation of this was provided in Govardhan and Williamson (2006), where the peak transverse amplitude of an elastically mounted cylinder was nearly unaffected as the aspect ratio varied between 7.2 and 22.7. The same authors found that blockage had no effect either on the amplitude response between 5% and 14%. Our blockage ratio is 10%.

Measurements of the natural frequency in air f_{Nv} and the damping ratio ζ are reported in the Appendix. The relatively high structural damping is due to the mechanical friction of the metal strip inside the torsion springs (see Fig. 2). A total spring constant of $35.3\,\mathrm{N\,m^{-1}}$ was measured during decay tests in air. The structural characteristics of the system are summarized in Table 2, in the Appendix.

2.2. Cylinder motion measurements

The amplitude and frequency of the system response were investigated for reduced velocities ranging from 4.8 to 6.9. Corresponding Reynolds numbers span from 13 000 to 18 600. In this range of U^*, the cylinder experienced a two-dimensional motion along the X and Y axes with only weak roll and pitch motions, as documented below. The limits regarding the range of investigation were imposed by the mounting itself. For U^* below 4.8, self-induced oscillations were intermittent, due to the high resistance of the plate springs. On the other hand, for reduced velocities exceeding 7, the cylinder experienced a significant roll motion leading to contacts with the supporting plates.

The cylinder trajectory was obtained from video recordings, using a camera towed along with the rig. The camera was placed with an angle to the cylinder axis in order to track simultaneously the displacement at both extremities. Following the initial acceleration of the rig, stable oscillations were observed after a short transient phase, typically 10 periods long. For each towing speed, three runs were performed providing around 40 cycles of periodic motion.

A comparison of the vertical and horizontal displacement at the two ends is presented in Fig. 3 for $U^* = 5.9$. The extremities of the cylinder are moving almost in phase and with similar amplitudes, showing that the cylinder motion is essentially two-dimensional. The average phase lag between the vertical displacement at each end is comprised between 2% and 3% of the period of oscillation. For U^* in the range 4.8–6.9, the peak value of the phase lag is up to 10% (see Fig. 4(b)). Although the set-up allows rotations around the X and Y axes, these motions are thus marginal compared to the main oscillations in the vertical plane. One can conclude that for the range of velocities concerned, the hydrodynamic forcing is well correlated along the span.

The cylinder amplitude of motion was calculated at mid-span by averaging the data from the two cameras:

$$A_y^* = \frac{y_1 + y_2}{2d}, \quad A_x^* = \frac{x_1 + x_2}{2d},$$

where (x_1, y_1) and (x_2, y_2) denote the amplitudes at extremities 1 and 2, respectively. The standard deviation of A_y^* (in % of the mean value) is plotted in Fig. 4(a). A high variability was recorded at the lower speeds due to the important friction produced by the plate springs. As the hydrodynamic forcing increases and the system gains momentum, the standard deviation drops down to 5% between $U^* = 5.5$ and 6.1. The cylinder oscillations become less regular as U^* approaches 7, an observation that can be related to the occurrence of roll motion for higher speeds.

2.3. PIV set-up

A two-dimensional PIV technique was used to extract the flow velocity field in a vertical plane situated at mid-span. Images were obtained with a Photron APX CMOS camera coupled with a pulsed Nd:YAG laser, at 10 ms interval, which yielded a particle displacement of 6–9 pixels between two subsequent images. The MatPIV software, described in Sveen (2004), used a discrete window-offset algorithm with two passes to cross-correlate the images, ending with 32×32 pixels subwindows. The cylinder section was masked during the cross-correlation step. An accuracy of less than 0.1 pixels (2%) is expected for the velocity, and 10% for the vorticity, although these values should be affected in regions of the flow presenting high velocity gradients; see e.g. Scarano (2002).

A 50% overlapping between the subwindows yielded a spatial resolution of 4 mm. The vorticity field was computed using a centred three-points scheme. The PIV system was fixed with respect to the tank, so that for each run about half a cycle of motion only was recorded. On the other hand, the light sheet characteristics (width, mirror alignment, angle to the flow) could be carefully tuned and maintained during the experiments.

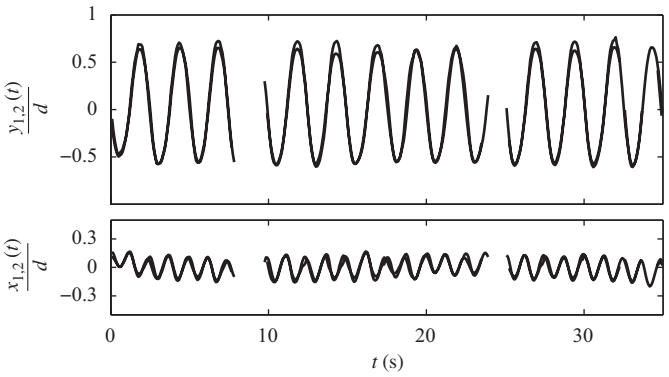

Fig. 3. Time traces of the displacement at the extremities of the cylinder, for $U^* = 5.9$.

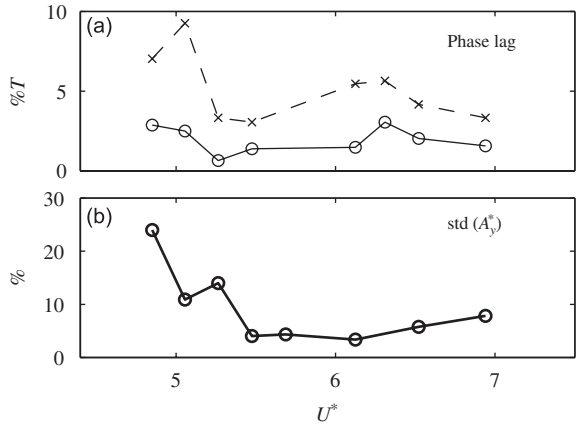

Fig. 4. (a) Phase lag between the vertical displacements at the two extremities, expressed as a percentage of the oscillation period T. ○, mean value over all runs; ×, peak values. (b) Standard deviation of the vertical amplitude of motion at mid-span, for each reduced velocity investigated.

3. Results

3.1. $X-Y$ trajectories

A good approximation of the in-line and transverse displacements at mid-span is provided by the following equations:

$$x(t)/d = A_x^* \sin(4\pi f_{ex} t + \theta), \quad y(t)/d = A_y^* \sin(2\pi f_{ex} t),$$

where the quantities are defined in Table 1. The $X-Y$ trajectory shapes plotted in Fig. 5 superpose all data available at these speeds and were used to estimate the phase angle θ between the in-line and transverse motions.An 80° shift exists with the results by Jauvtis and Williamson (2004). The difference is striking when comparing the actual shape of the cylinder path at the peak transverse amplitude: while the above-mentioned authors report a crescent pattern, we observe a figure-of-eight with large lobes. These observations reflect the difference in the timing of the vortex shedding in the two cases, and are further discussed in Section 4.

The periodicity of the oscillations at different reduced velocities can be described in a qualitative way by observing the actual cylinder path. At $U^* = 5.1$ and 5.7 the repeatability is good, but at $U^* = 6.5$ the cylinder trajectory exhibits more variability. As pointed out in Fig. 4, changes in the amplitude and (to a lesser extent) the shape occur from one cycle to the other. The periodicity of oscillations continues to deteriorate as the reduced velocity is increased beyond 6.5. A significant roll motion appears for U^* exceeding 7.

Table 1
Definitions

X	Streamwise (horizontal) direction
Y	Transverse (vertical) direction
$x(t)$, $y(t)$	Cylinder displacement at mid-span
$A^*_{x,y}$	Normalized amplitude of oscillation at mid-span
m^*	Ratio of oscillating mass over displaced mass
k, b	Spring and damping constant in both directions
m_A, C_A	Potential added mass and added mass coefficient ($C_A = 1$)
$\zeta = \dfrac{b}{2\sqrt{k(m+m_A)}}$	Damping ratio
$\alpha = (m^* + C_A)\zeta$	Combined mass-damping parameter
f_{ex}	Vibration frequency
$f_{Nw} = \dfrac{1}{2\pi}\sqrt{\dfrac{k}{m+m_A}}$	Natural frequency in still water
$f_{Nv} = \dfrac{1}{2\pi}\sqrt{\dfrac{k}{m}}$	Natural frequency in vacuum
$f^* = \dfrac{f_{ex}}{f_{Nw}}$	Reduced vibration frequency
f_s	Strouhal frequency
$U^* = \dfrac{U}{f_{Nw}d}$	Reduced velocity in water

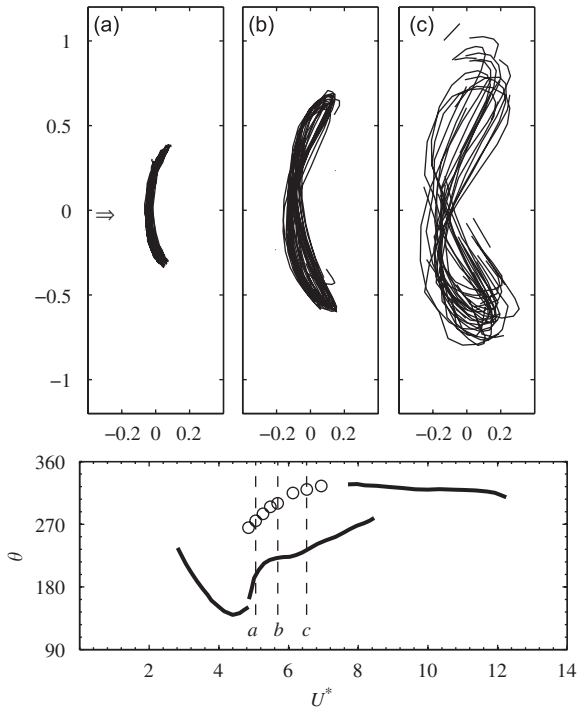

Fig. 5. Top: trajectory shapes corresponding to $U^* = 5.06$, 5.69 and 6.52; the arrow indicates the direction of the flow relative to the carriage. Bottom: phase angles between X and Y motion (○), compared to the results by Jauvtis and Williamson (2004) (thick line).

Also visible in Fig. 5 (for $U^* = 5.69$) is the slight asymmetry between the lobes of the figure-of-eight, whose origin is discussed in Section 2.1. As a consequence, we observed that the vortex shed from the lower shoulder of the cylinder is slightly stronger than its counterpart at the upper one. However, we believe that this does not affect the main conclusions presented here.

3.2. Amplitude and frequency response

The amplitude, computed by the average of the top 10% values of A_y^* and A_x^* recorded at each speed, and frequency response are plotted in Fig. 6. We compare our data to the low mass-ratio case in Jauvtis and Williamson (2004), hereafter denoted by JW (2004). Their mass-damping parameter and Reynolds number are different with $\alpha = 0.013$ and $\mathrm{Re} \simeq 5800$ at maximum response, while we have $\alpha = 0.093$ and $\mathrm{Re} \simeq 18\,600$. Mass ratios are close with $m^* = 2.6-1.04$, and in both experiments the natural frequency and the oscillating mass are equal in the X and Y directions. The amplitude response in JW (2004) for a moderate mass ratio $m^* = 7.0$ is also shown to illustrate the difference with the low mass-ratio case in their experiments.

We observe that the peak transverse amplitude measured in our experiments is 50% lower than the top of the super-upper branch in JW (2004) (Fig. 6). The reason for this discrepancy is analysed in Section 4 in light of the recent work by Govardhan and Williamson (2006). However, in the horizontal direction the amplitude response is similar ($A_x^* \simeq 0.3$). The in-line motion is thus proportionally larger in our experiments, with A_x^*/A_y^* reaching 0.28, against 0.2 for JW (2004).

The frequency response suggests that all points of measurements belong to the same branch, with f^* increasing continuously from 0.85 ($U^* = 4.8$) to 1.16 ($U^* = 6.9$). Flow visualizations (see Section 3.3) show that the vortex regime corresponds to the initial branch. In agreement with the results reported for systems characterized with a high mass-damping parameter (e.g. Feng, 1968), the amplitude is expected to drop to the lower branch for higher reduced velocities. The transition coincides with a 'jump' in the frequency response across the natural frequency in water and a shift in the mode of vortex formation (Govardhan and Williamson, 2000), from the '2S' to the '2P' regime.

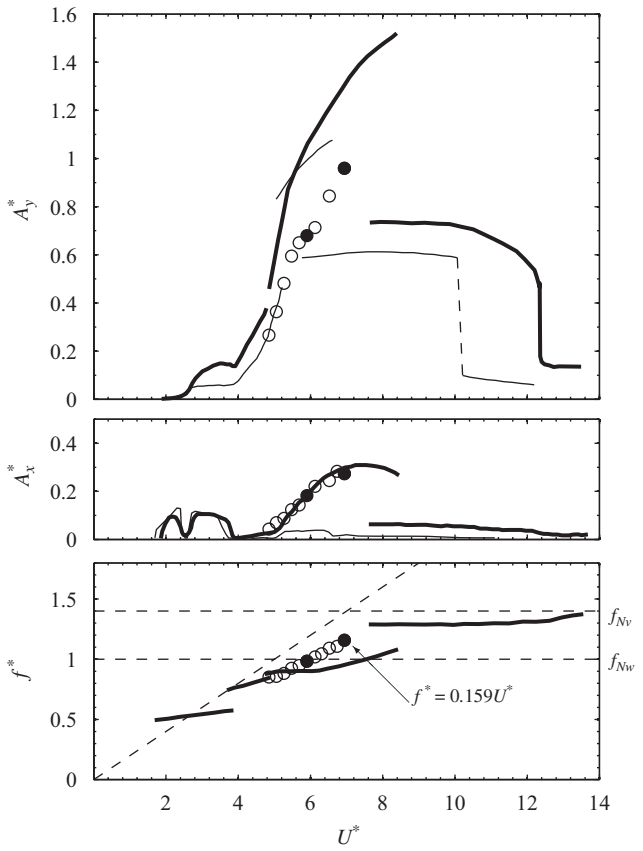

Fig. 6. Response of the system compared with the results by Jauvtis and Williamson (2004) (thick line: $m^* = 2.6$, $\alpha = 0.013$; thin line: $m^* = 7.0$, $\alpha = 0.012$). Top: amplitudes of motion in the transverse and horizontal directions. Bottom: frequency response. The values corresponding to the natural frequencies in water and vacuum are indicated, as well as the Strouhal frequency (oblique, dashed line). Black symbols refer to points where PIV flow measurements are shown.

Interestingly, in the results reported in Fig. 6, f^* passes continuously across 1. In the JW (2004) study, the transition in vortex regimes occurs between $f^* = 0.8$ and 0.9, while in our case the initial branch persists beyond $f^* = 1.16$.

A linear fit of the frequency response in the range $U^* = 5-7$ shows that $f^* \simeq 0.159 \times U^*$ for our data. For transverse-only oscillations and under conditions of low mass-damping, Govardhan and Williamson (2000) showed that the reduced frequency increased linearly with U^* in the upper branch, until the system reached the lower branch. They derived an experimental relation predicting the position of the lower branch, and thus the slope of f^* versus U^* in the upper branch, as a function of the mass ratio. For $m^* = 1.05$ they found a slope of 0.154. This is remarkably close to our value, in spite of the important differences between the two mechanical systems. The agreement suggests that their conclusions can be extended to the initial branch for systems with a high mass-damping parameter and a low mass ratio.

3.3. Flow visualization

PIV data were collected for reduced velocities of 4.4, 4.7, 5.1, 5.9, 6.6 and 6.9. Instantaneous velocity fields for $U^* = 5.9$ and 6.9 are presented in Figs. 7 and 8 with the cylinder halfway between the top and bottom positions, moving

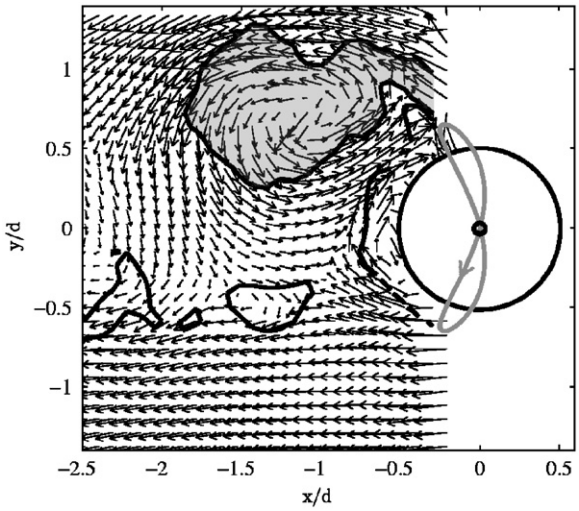

Fig. 7. PIV velocity field at $U^* = 5.9$ with the cylinder at the middle position, moving downwards. Vorticity contours correspond to $\omega d/U = \pm 2.5$. Relative to the towing tank carriage, direction of the flow is from right to left.

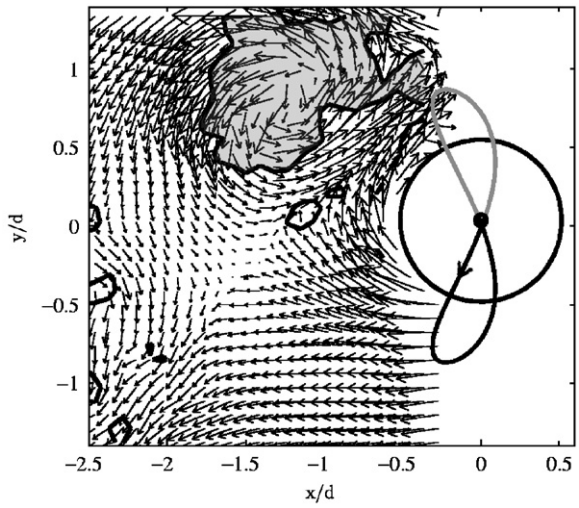

Fig. 8. Same as Fig. 7, for $U^* = 6.9$.

downwards. In both figures a strong vorticity concentration indicates the position of the primary vortex originating from the roll-up of the upper shear layer. Relating these pictures to the extensive descriptions of the '2S' and '2P' modes found in Govardhan and Williamson (2000) for transverse-only motion, or Jeon and Gharib (2001) for forced 2-dof vibrations, we clearly identify a 2S pattern for all reduced velocities investigated with PIV. This observation brings evidence that the response branch described in Fig. 6 corresponds to the initial branch.

One of the observations drawn from the study by Jeon and Gharib (2001) is that the addition of streamwise motion to their forced oscillations greatly increased the coherence of the vortices in the 2S case. This might explain the clarity of the vortical structures shown in Figs. 7 and 8, keeping in mind that these are instantaneous flow fields obtained at a Reynolds number of 15 000.

4. Discussion and conclusion

A compact and simple mounting has been developed to study VIV of a rigid, elastically mounted cylinder in two degrees of freedom, with equivalent mass ratio and natural frequency in the two directions of motion. The relevant parameters are $m^* = 1.04$, $\alpha = 0.094$ and $\mathrm{Re} = 18\,600$ at maximum response.

The combination of a very low mass ratio and high structural damping leads to interesting observations: while the amplitude response seems to correspond to 'high mass-damping' systems where the upper branch is absent and the peak amplitudes are obtained in the initial branch, the frequency response shows strong similarities with the 'low mass-damping' description. The linear relation between f^* and U^* that characterizes the upper branch in the study by Govardhan and Williamson (2000) holds here for the initial branch, with the slope corresponding very well for equal mass ratios. For transverse oscillations only, Govardhan and Williamson (2006) stated that the condition $A^* = 0.6$ may be used to separate the regimes of three-branch and two-branch responses over a wide range of Reynolds numbers (from 100 to 100 000). However, the amplitude response data presented here suggest that even with A_y^* up to 0.9 we obtain a two-branch response.

Another feature of the present mounting is that rotations around the X and Y axes are not restricted. Below $U^* = 6.5$, the rolling motion was barely visible and did not seem to affect in any way the main $X-Y$ oscillations. From $U^* = 6.5$ and up to the maximal reduced velocity investigated ($U^* = 6.9$), the cylinder started to experience significant roll at intervals, corresponding to a drop in the transverse amplitude. These events became more frequent and stronger as the reduced velocity increased, and we stopped when the cylinder started to hit the supporting plates placed at each side. The investigation by Hover et al. (1998) sheds some light on this point. They studied the correlation between the forces measured at the two ends of freely vibrating or forced cylinders, and reported a loss of correlation in the range separating the 2S mode from the 2P mode of vortex formation. Following the results obtained in Techet et al. (1998) for tapered cylinders, they concluded that this is due to a spanwise transition between the two modes, with the intermittent appearance of hybrid 2S–2P structures along the span. This loss of flow correlation, as the system approaches the 2S–2P transition, will in our case trigger the onset of roll motion and disrupt the $X-Y$ oscillations.

Although the limited range of reduced velocities investigated did not allow us to cover the totality of the initial branch, we can assume that the last measurement point in Fig. 6 ($U^* = 6.9$) is close enough to the initial-lower branch transition to report this value in the Griffin plot in Fig. 9, along with classical results for different parameters and configurations.

With respect to the combined mass-damping parameter α, the present result is situated in-between the ranges investigated by Feng (1968) and Khalak and Williamson (1999) for transverse-only oscillations. In the case of two-degree-of-freedom motion, Jauvtis and Williamson (2004) (JW 2004) made a distinction between moderate mass ratios ($m^* > 6$), with peak amplitudes corresponding to the transverse-only results, and low mass ratios ($m^* < 6$) yielding extreme peak amplitudes up to 1.5 diameters in the 'super-upper' branch. The difference is illustrated in Fig. 6.

To compare our results, it is necessary to take into account the difference in Reynolds number (Govardhan and Williamson, 2006). In Fig. 9 our maximum amplitude lies far above the results by JW (2004) obtained at moderate mass ratios and similar mass-damping, thereby suggesting that the peak transverse amplitude is actually increased by the combination of a low mass ratio and two-degree-of-freedom oscillations. However, in the 'modified' Griffin plot introduced by Govardhan and Williamson (2006), the difference vanishes and our data actually fall under the functional representation of the modified amplitude A_M^* (independent of Reynolds number) versus α (Fig. 10). The peak amplitude is comparable to the transverse-only case, although our mass ratio is less than 6. In the JW (2004) study the 'super-upper' branch is associated with a modification of the vortex dynamics. Instead of the classical 2P mode usually found in the upper branch for a low mass-damping type of response, they observed a new mode of vortex formation with triplets of vortices emitted during half a cycle of motion ('2T' mode). In addition to the primary vortex originating

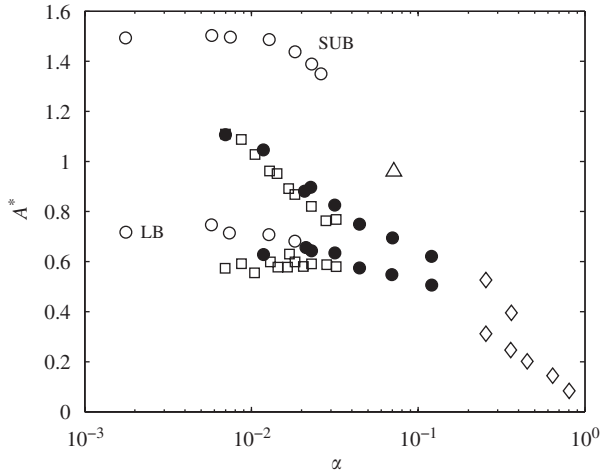

Fig. 9. 'Griffin' plot, for transverse-only and 2-dof results. △, Present result; ◇, Feng (1968); □, Khalak and Williamson (1999); ○, Jauvtis and Williamson (2004), for low mass ratios, 2-dof (SUB = 'super-upper branch', LB = 'lower branch'); •, Jauvtis and Williamson (2004), for moderate mass ratios, 2-dof.

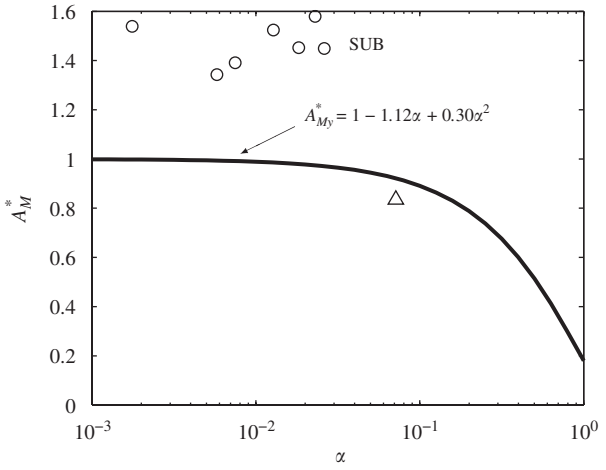

Fig. 10. Modified 'Griffin' plot taking into account the effect of Reynolds number. △, Present result; ○, super-upper branch from Jauvtis and Williamson (2004); −, functional relation between A^*_M and α proposed by Govardhan and Williamson (2006).

from the roll-up of the shear layer, each triplet consisted of a pair of counter-rotating 'starting vortices' created by the sudden acceleration of the cylinder as the body moves from the extreme positions towards the centre. Obviously, such a change in the vortex shedding cannot occur here because the maximum amplitudes are obtained in the initial branch, associated with the 2S mode. Our conclusion is that for systems characterized by a high mass-damping type of response, the ability to move in-line and cross-flow with a very small mass ratio $m^* \simeq 1$ does not affect dramatically the transverse response.

Finally, in Fig. 11 the response amplitude presented in Fig. 6 is plotted versus the normalized velocity $(U^*/f^*)S$, with the map of vortex regimes by Williamson and Roshko (1988). This choice of parameter allows sets of data obtained with different mass ratios to collapse together. The presence of all our measurement points (forming the initial branch) in the 2P area of the Williamson and Roshko map requires some explanation. Govardhan and Williamson (2000) made a similar observation in their high mass-damping case obtained with $500 < \mathrm{Re} < 4000$. They noted that the boundaries between vortex regimes might need to be shifted to take into account the difference in Reynolds number: the map was drawn from the observation of the wake behind a cylinder at Reynolds numbers between 300 and 1000. The same argument holds in the present experiments where $13\,000 < \mathrm{Re} < 18\,600$.

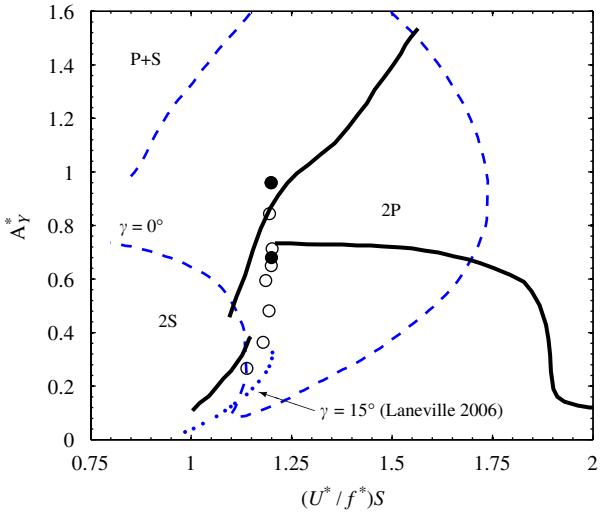

Fig. 11. Transverse amplitude response versus normalized velocity $(U^*/f^*)S$. Labels: see Fig. 6. The Williamson and Roshko map of vortex regimes is superimposed in dashed line. The dotted line represents the critical curve by Laneville (2006) for $\gamma = 15^\circ$.

Secondly, a recent paper by Laneville (2006) has pointed out the influence of streamwise motion on the critical curve separating the 2S from the 2P regimes in the Williamson and Roshko map. Based on the experiments by Brika and Laneville (1995) for a flexible cylinder in an airflow where the plane of vibration could be tilted, the author observed that the critical curve shifted towards higher reduced velocities as the tilting angle γ increased. For $\gamma > 30^\circ$, the 2P regime even ceased to exist. In the case of freely vibrating rigid cylinders with two degrees of freedom and with the same natural frequency in both directions, $\tan\gamma = A_x/A_y$ yields $\gamma = 16^\circ$ in the present experiments. The critical curve found in Laneville (2006) for $\gamma = 15^\circ$ has been added to Fig. 11. According to the new 2S/2P separation, the lower part of the response branch described here (up to $U^* = 5$) now falls into the 2S area, in agreement with our PIV observations. Unfortunately, the critical curves presented in Laneville (2006) are restricted to amplitudes smaller than 0.4.

Acknowledgements

The assistance with PIV by Atle Jensen and with the laboratory set-up by Arve Kvalheim and Svein Vesterby is gratefully acknowledged. This work was funded by the Norwegian Deep Water Program and the Strategic University Program, Modelling of currents and waves for sea structures 2002-6, NFR 146526/420.

Appendix

Free decaying tests in air were performed to determine the structural damping and the effective spring constant of the system. The cylinder was filled with water and sealed, in order to reach the same oscillating mass as when it is submerged. It was then suspended to the ceiling with 2.8 m long cables to withstand the weight and allow for horizontal oscillations (see Fig. 12).

The motion of the cylinder, displaced from the position of equilibrium by a distance y_0 and then released, obeys the following equation (for small oscillations):

$$m\ddot{y} + b\dot{y} + \left(k + \frac{mg}{l}\right)y = 0, \tag{A.1}$$

neglecting dissipation in the pendulum itself. The envelope of maxima is given by: $y_{\max} = y_0\, e^{-\beta\omega_0 t}$, where the following expressions have been used: $\omega_0 = \sqrt{k'/m}$, $k' = k + mg/l$ and $\beta = b/2m\omega_0$.

y_0 varied from 5.5 to 10 cm during the decay tests to cover the cylinder excursions in the experiments. β is calculated by plotting $\ln(y_{\max})$ as a function of time and measuring the slope, while ω_0 is directly measured from the decay tests since $\beta^2 \ll 1$ ($\beta = 0.052-0.067$).

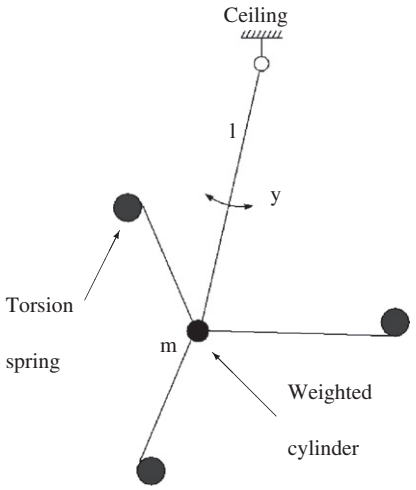

Fig. 12. Side view of the set-up used for decay tests in air.

Table 2
Characteristics of the oscillating system

Cylinder dimensions (cm)	$d = 8$, $L = 47.5$
m (kg), m^*	2.49, 1.04
k ($\mathrm{N\,m^{-1}}$)	35.3 ± 0.3
f_{Nw}, f_{Nv} (Hz)	0.42, 0.60
b ($\mathrm{kg\,s^{-1}}$)	1.25 ± 0.15
ζ	0.046 ± 0.005

Due to the strong energy loss in the springs, the range of exponential decay is limited to the three or four first maxima, after which the oscillations become dominated by the effect of Coulomb-type friction in the springs. As a result, the uncertainty for the damping b is high. The measured values of k and b are $k = 35.3 \pm 0.3\,\mathrm{N\,m^{-1}}$ and $b = 1.25 \pm 0.15\,\mathrm{kg\,s^{-1}}$, see Table 2.

References

Brika, D., Laneville, A., 1995. An experimental investigation of the aeolian vibrations of a flexible circular cylinder at different incidences. Journal of Fluids and Structures 9, 371–391.

Feng, C.C., 1968. The measurements of vortex-induced effects in flow past a stationary and oscillating circular and d-section cylinders. Master's Thesis, University of British Columbia, Vancouver, BC, Canada.

Govardhan, R., Williamson, C.H.K., 2000. Modes of vortex formation and frequency response for a freely-vibrating cylinder. Journal of Fluid Mechanics 420, 85–130.

Govardhan, R., Williamson, C.H.K., 2006. Defining the 'modified Griffin plot' in vortex-induced vibration: revealing the effect of Reynolds number using controlled damping. Journal of Fluid Mechanics 561, 147–180.

Hover, F.S., Techet, A.H., Tryantafyllou, M.S., 1998. Forces on oscillating uniform and tapered cylinders in crossflow. Journal of Fluid Mechanics 363, 97–114.

Jauvtis, N., Williamson, C.H.K., 2004. The effect of two degrees of freedom on vortex-induced vibration at low mass and damping. Journal of Fluid Mechanics 509, 23–62.

Jeon, D., Gharib, M., 2001. On circular cylinders undergoing two-degree-of-freedom forced motions. Journal of Fluids and Structures 15, 533–541.

Khalak, A., Williamson, C.H.K., 1999. Motions, forces and mode transitions in vortex-induced vibrations at low mass-damping. Journal of Fluids and Structures 13, 813–851.

Klamo, J.T., Leonard, A., Roshko, A., 2006. The effects of damping on the amplitude and frequency response of a freely vibrating cylinder in cross-flow. Journal of Fluids and Structures 22, 845–856.

Laneville, A., 2006. On vortex-induced vibrations of cylinders describing x–y trajectories. Journal of Fluids and Structures 22, 773–782.

Moe, G., Wu, Z.J., 1990. The lift force on a cylinder vibrating in a current. ASME Journal of Offshore Mechanics and Arctic Engineering 112, 297.

Pesce, C.P., Fujarra, A.L.C., 2002. Vortex induced vibrations experiments with an elastically mounted cylinder in water. In: Proceedings of the 12th International Offshore and Polar Engineering Conference (ISOPE). KitaKyushu, Japan, pp. 502–509.

Pesce, C.P., Fujarra, A.L.C., 2005. The 'super upper branch' VIV response of flexible cylinders. In: Leweke, T., Williamson, C.H.K. (Eds.), Proceedings of the 4th Symposium on Bluff Body Wakes and Vortex-Induced Vibrations (BBVIV-4). Santorini, Greece, pp. 275–276.

Sarpkaya, T., 1995. Hydrodynamic damping, flow-induced oscillations and biharmonic response. ASME Journal of Offshore Mechanics and Arctic Engineering 117, 232.

Scarano, F., 2002. Iterative image deformation methods in PIV. Measurement Science and Technology 13, R1–R19.

Sveen, J.K., 2004. An introduction to MatPIV v.1.6.1. E-print no. 2, ISSN 0809-4403, Department of Mathematics, University of Oslo. ⟨http://www.math.uio.no/ ~jks/matpiv⟩.

Szepessy, S., Bearman, P.W., 1992. Aspect ratio and end plate effects on vortex shedding from a circular cylinder. Journal of Fluid Mechanics 234, 191–217.

Techet, A.H., Hover, F.S., Tryantafyllou, M.S., 1998. Vortical patterns behind tapered cylinders oscillating transversely to a uniform flow. Journal of Fluid Mechanics 363, 79–96.

Tryantafyllou, M.S., Hover, F.S., Techet, A.H., 2004. High Reynolds number test results. Workshop on Vortex Induced Vibrations. Trondheim, Norway.

Williamson, C.H.K., Govardhan, R., 2004. Vortex-induced vibrations. Annual Review of Fluid Mechanics 36, 413–455.

Williamson, C.H.K., Roshko, A., 1988. Vortex formation in the wake of an oscillating cylinder. Journal of Fluids and Structures 2, 355–381.